MOSAIC: Simultaneous Localization and Environment Mapping using mmWave without a-priori Knowledge

Ali Yassin[1], Youssef Nasser[1], Ahmed Al-Dubai[2], Mariette Awad[1]

[1]Department of Electrical and Cmputer Engineering, Maroun Semaan Faculty of Engineering and Architecture, American University of Beirut, Lebanon

[2]School of Computing, Edinburgh Napier University Edinburgh, Scotland, United Kingdom

Abstract—Simultaneous Localization and environment mapping (SLAM) is the core to robotic mapping and navigation as it constructs simultaneously the unknown environment and localizes the agent within. However, in millimeter wave (mmWave) research, SLAM is still at its infancy. In this paper, we introduce MOSAIC a new approach for SLAM in indoor environment by exploiting the map-based channel model. More precisely, we perform localization and environment inference through obstacle detection and dimensioning. The concept of Virtual Anchor Nodes (VANs), known in literature as the mirrors of the real anchors with respect to the obstacles in the environment, is firstly introduced. Then, based on these VANs, the obstacles positions and dimensions are estimated by detecting the zone of paths obstruction, points of reflection and obstacle vertices estimation. Cramer-Rao Lower Bounds (CRLB) are then derived to find the optimal number of anchor nodes and measurements points that improve the localization and mapping accuracy. Simulation results have shown high localization accuracy and obstacle detection in different environments using mmWave technology.

Index Terms—Millimeter wave, Triangulateration (TL), Angle-Difference-of-Arrival (ADoA), Virtual Anchor Node (VAN), Simultaneous Localization and Mapping, Obstacle Detection.

I. Introduction

MilliMeter Wave (mmWave) wireless communication systems have recently gained great research interests due to their benefits in terms of spectrum, propagation characteristics, potential applications and services [1][2]. The shortness of the coverage range of anchor nodes (ANs) operating at mmWave frequencies triggers the deployment of a capillary network of ANs in the buildings offering enhancements in terms of localization. Among the potential services offered by mmWave, localization and mapping appear as key factors in enabling new means and tools for communications systems [3], particularly indoor positioning systems (IPS).

Recently, IPS have been at the center of attention for researchers because of the vast technological enhancement in smart phones and tablets, and the evolving technology of Internet of Things (IoT) as a future service in 5G. For instance, localization is critical for detecting products stored in a warehouse, medical equipment and personnel in a hospital, firemen in a building with fire, etc. With the evolution of mmWave communication systems, IPSs will exploit the infrastructure of future mmWave groundwork.

In literature, there exist few researches on localization systems operating at mmWave frequencies. Most of the research work was focused on measuring the delay spread, Time-of-Arrival (ToA), Time-Difference-of-Arrival (TDoA) and Angle-of-Arrival (AoA) methods [4][5].

The channel characteristics at the mmWave frequencies differ from low frequencies range in many aspects; hence, the exploitation of these characteristics for localization and mapping should be totally revised and new approaches are to be proposed. At the same time, these properties open the door for additional applications such as mmWave based radar systems. Indeed, researches have shown that the channel at mmWave behaves as quasi-optical channel in which the Line of Sight (LoS) ray is dominant. Moreover, it has been shown that the channel power exponentially decays in None-Line-of-Sight (NLoS) environment where a single-bounce is usually carrying most of the power. On the other hand, the characteristics of the channel at those frequencies showed that reflections don't generate significant amount of scattering [7], and that the transmitted beam will have the same directivity after reflections with slight scattering [8]. Hence, Snells law holds in terms of the equality between the angles of departure and incidence upon reflection [9]. As a consequence, these propagation characteristics make the localization and mapping a very challenging task at mmWave. The appropriate localization procedures and mapping approaches should be then derived [10][11][12].

Originally, the concept of Simultaneous Localization and Mapping (SLAM) was achieved (in robotics) by moving a robot in an unknown environment to be recognized. The process is based on steering a laser beam across a dense number of test directions. Then, the round-trip time (RTT) of the signal reflected by the obstacles is estimated in each direction. Hence, the distance to obstacles, inferred from the RTT, was used to build the indoor map. Accurate ranging and high angle resolution are the two main inputs for an accurate SLAM. Such aspects were usually achieved through laser technology. Nevertheless, as the technology has to be equipped with laser and mechanical steering devices it is considered to have a complex and high-cost integration in mobile devices [13][14]. At mmWave frequencies, very few works have dealt

with SLAM approaches. We particularly mention the works of [15] and [16] where the authors proposed a radar-based system operating at mmWaves to overcome the shortcomings of laser. They provided high ranging accuracy using wideband signals and high directional antenna with mechanical steering. Technically, the reflected signal from the obstacle is scanned in front of the radar transceiver to estimate the distance from the obstacle. Thanks to the large system bandwidth and high temporal resolution of the paths, the proposed approaches therein have shown high accuracy. However, the system has to be in radar-like configuration, i.e. perpendicular to the obstacle, in order to have highly accurate mapping. We should mention that this radar-like system was possible in mmWaves as the latter promotes the implementation of massive antenna arrays at the ANs [17]-[20]. This is indeed possible due to the reduced size of antenna arrays. For instance, the works in [21]-[24] proposed new designs of personal radar with SLAM features using massive antenna arrays placed in a smart-phone or tablet. Likewise, the authors of [25] adopted mmWave technology with multi-antenna radar system to scan the environment even if the smart-phone is kept in the user pocket. The concept of SLAM is expected to be widely spread in the future, especially in the domain of IoT [26].

In this paper, our approach for SLAM in mmWave technologies is totally different. The proposed work does not impose any constraint on the receiver orientation and configuration; rather, it exploits the rays characteristics and the separation capabilities of these rays at the receiver to propose an innovative framework (called MOSAIC) for localization and mapping purposes. More precisely, the paper exploits one or more of the localization metrics, i.e. AoA, ToA, and RSS, to achieve the Obstacle Detection, mapping and dimensioning. The latter are assumed to have different shapes and randomly distributed in the indoor environment. Throughout the paper, the system model is firstly derived for one AN and one receiver and then extended to multiple ANs. The number of ANs has been optimized through Cramer-Rao Lower Bounds (CRLB) derivations. The CRLBs outcomes are then used in the simulations to assess the proposed localization and mapping approaches.

Technically speaking, we will briefly introduce a first approach available in literature on the localization of a receiver (Rx) in a known environment using the concept of virtual anchor nodes (VANs). Then, as shown in Fig. 1, the concept of Rx localization is extended to unknown environment. In this case, MOSAIC proposes to exploit the information obtained by at least two channel metrics (ToA, AoA, RSS) to estimate the RX position. To implement a joint localization and mapping, MOSAIC is based on the estimation of the VANs positions, followed by the estimation of the obstacles sides directions and positions. Then, MOSAIC proposes two approaches for the obstacles dimensions (i.e. sides).

This paper extends our previous work in [29] in which the room geometry has been identified using the AoA metric only. The contributions of this paper could be summarized as follows:

- Exploitation of the map-based mmWave channel characteristics to provide localization and mapping in indoor scenarios.

- Extension of our previous work in [29] based on AoA metrics to other metrics (RSS and TDoA): this extension is needed since in real scenarios these channel metrics are available and could be exploited to improve the localization and mapping accuracy
- Exploitation of the VANs principle widely used in literature to realize the obstacle positioning, dimensioning and mapping. In the paper, MOSAIC proposes two different approaches for mapping. The first one is based on estimating the cloud of reflection points (CoRP) belonging to the obstacle borders. The CORP will be used to estimate the obstacles limits, positions and dimensions. The second is based on determining the obstacles vertices.
- Derivation and exploitation of the CRLB to optimize the number of anchor nodes (ANs) needed to achieve a target accuracy.
- Validation of proposed approaches through extensive simulation results.
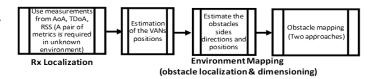

Fig. 1. Steps needed in MOSAIC

The rest of this paper is organized as follows. In Section 2, we develop the system model and the localization methodology of the receiver using mmWave. In Section 3, we introduce localization approaches in mmWave with an extension to unknown environment. In section 4, we propose new approaches for context inference by estimating obstacles positions and dimensions. In Section 5, the effect of the number of ANs is discussed using the CRLB. Then, we provide in section 6 the simulation results for an indoor environment, while conclusions are drawn in Section 7.

II. MOSAIC: System Model and Environment

A. System Environment

We consider in this paper a 2D indoor environment consisting of a room bounded by 4 walls for the sake of simplicity. The extension to 3D environment is left for further work. The room geometry is assumed to be known with single transmitter and single receiver. This assumption does not change any step in the proposed approaches neither in the conclusions but makes the model simpler to argue. The room boundaries and radio-reflective obstacles in the reflective objects are grouped in a set O. Obstacles are described as two-dimensional flat polygonal faces with sharp vertices and straight edges. Each oriented obstacle S is denoted by its perpendicular line, described by:

$$y = p_y + \alpha * (x - p_x) \tag{1}$$

where $\mathbf{p} = (p_x, p_y)$ is a point of intersection between the obstacle and its perpendicular and α is the slope of the line orthogonal to the obstacle S. By assumption, a single mmWave transmitter (Tx) is deployed in the room at a location $\mathbf{p}^{Tx}$.

Additionally, the transmitter is assumed to broadcast its position to the node(s) targeted for localization.

Throughout the paper, AoA will be the main metric for localization and mapping. It is very robust against power loss and absorption at mmWave [27]. The AoA spectrum has been widely used in literature. It gives the power received at each angle of arrival hence it is usually modeled as a $2 \times N_p$ matrix, $SP_p(\theta)$, that records the amplitude of each received ray component (RRC) as a function of the azimuth θ at a given location $\mathbf{p}$, where N_p is the number of RRCs. Each RRC can be either due to a LoS link between the transmitter and the receiver or due to NLoS link caused by reflections of one or more surfaces in the obstacle set O. Localization in this case is achieved by observing NLoS paths as virtual LoS rays coming through virtual LoS links from VANs. A sorting in decreasing order of $SP_p(\theta)$ according to the first row, i.e. to ray power, allows to characterize the received signal in which the first column has the highest power. In practice, if the receiver and transmitter are in LoS, this column represents θ_0, the AoA of the LoS ray, and its corresponding power. The columns $2 : N_p$ represent the NLoS paths.

B. Virtual Anchors

The concept of VAN in mmWaves has been introduced in literature [28]. As shown in Fig. 2, it is based on the fact that each NLoS ray is emitted from a virtual anchor node placed at the mirror position of the transmitter with respect to the reflector. In LoS conditions, we might have $(N_p - 1)$ RRCs that correspond to NLoS paths. The locations of the VANs are determined by mirroring the transmitter $\mathbf{p}^{Tx}$ with respect to the surfaces in the obstacle set O since it is the source of signal reflections. We denote $V = \{v_0, v_1, \ldots\}$ to be the set of the positions of all possible VANs, and we denote $\overline{V} = \{V_0, V_1, \ldots\}$ to be a partition of V as follows. We let $V_0 = \mathbf{p}^{Tx}$, and each set $V_i, i = 1, 2, \ldots$ represents all VANs that have been mirrored i times due to reflections caused by any surface in the obstacle set O [28]. Actually, there is no limit on the number of reflections of the signal transmitted by $\mathbf{p}^{Tx}$. However, a mmWave signal fades quickly during its propagation as it reflects off the surfaces. So, we limited the set $\overline{V}$ by assuming a maximum reflection order $\mu = 1$ in this paper[1]. Hence, the set of all VANs will be represented as $V_\mu = \bigcup_{i=0}^{\mu} V_i$. As shown in Fig. 2, the anchors v_i and v_j represent first and second order of reflection respectively; hence, $v_i \in V_1$ and $v_j \in V_2$. Nevertheless, we limited μ for single reflection.

III. LOCALIZATION USING MMWAVES

In this section, we consider a harsh environment with one Tx and one Rx only. We tackle the problem of localization in mmWave using AoA techniques due its robustness against power loss in mmWave [27]. The other conventional approaches such as TDoA and RSS could be also adopted but are not described in details for the sake of simplification. In this section and for the sake of clarification, we assume that the location orientation and dimensions of the obstacle are known at the

receiver. Hence, the target in this section is to introduce the localization techniques that are necessary for the mapping approaches proposed in unknown environment in the next section.
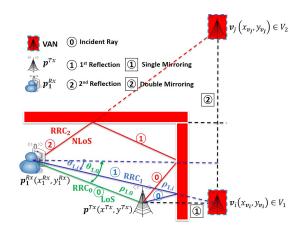

Fig. 2. VANs related to first and second order of reflections

A. The Triangulateration (TL) Algorithm in Known Environment: an AoA based Approach

This algorithm is based on estimating the location of a receiver at position $\mathbf{p}$ using a set of triangulation steps followed by a verification of the estimated positions [28][29].

The TL provides good accuracy with low complexity versus the conventional maximum likelihood (ML) algorithm[2]. TL steps are based on forming a triangle between the unknown receiver and each VAN. As shown in Figure 2, the following relations are constructed using trigonometric relations in the right triangle formed between the receiver and VAN $\mathbf{v}_i$ as follows:

$$x_{v_i} - x_1^{Rx} = \rho_{1,i} * \cos \theta_{1,i} \tag{2}$$

$$y_{v_i} - y_1^{Rx} = \rho_{1,i} * \sin \theta_{1,i} \tag{3}$$

where $\mathbf{v}_i = (x_{v_i}, y_{v_i})$ and $\mathbf{p}_1^{Rx} = \left(x_1^{Rx}, y_1^{Rx}\right)$ are the VANs and the unknown receiver respectively. $\theta_{1,i}$ and $\rho_{1,i}$ are the AoA and the distance of the RRC "transmitted virtually" from the VAN $\mathbf{v}_i$ to the receiver at position $\mathbf{p}_1^{Rx}$, respectively. In this section, we aim at estimating the position of the receiver, i.e. x_1^1 and y_1^{Rx} in (2) and (3). Hence, using $\theta_{1,i}$ and $\mathbf{v}_i$, the problem turns out to find $\rho_{1,i}$. The latter could be easily estimated by simply differentiating between the signal originated from different VANs. Hence, for each pair of VANs $\mathbf{v}_i$ and $\mathbf{v}_j$, the following equation holds:

$$\mathbf{V} = \mathbf{\Gamma}.\mathbf{P} \tag{4}$$

where $\mathbf{V}$, $\mathbf{\Gamma}$, and $\mathbf{P}$ are defined as follows:

$$\mathbf{V} = \begin{bmatrix} x_{v_i} - x_{v_j} \\ y_{v_i} - y_{v_j} \end{bmatrix}$$

$$\mathbf{\Gamma} = \begin{bmatrix} \cos \theta_{1,i} & -\cos \theta_{1,j} \\ \sin \theta_{1,i} & -\sin \theta_{1,j} \end{bmatrix}$$

---

[1] The number of reflections at mmWave is usually limited to 2 as the power is almost negligible afterwards. In this paper, $\mu = 2$ is left for further studies

[2] For a fair comparison, ML results will be provided in the simulations results section.

$$\mathbf{P} = \begin{bmatrix} \rho_{1,i} \\ \rho_{1,j} \end{bmatrix}$$

Solving (4), we obtain:

$$\mathbf{P} = \mathbf{\Gamma}^{-1}.\mathbf{V}_{i,j} \tag{5}$$

Knowing $\mathbf{P}$, the estimation of the position $\mathbf{p}_1^{Rx}$ of the receiver can be done by inserting $\rho_{1,i}$ in (2) and (3). The TL steps are repeated K times, that is the total number of all possible pairs of $(\mathbf{v}_i, \mathbf{v}_j)$, $i \neq j$ in the set V_1. So, we will obtain K estimates of the receiver position. The final estimate will be the average of all estimates $\mathbf{p}_k, k = 1, 2, \ldots K$.

B. TL Extension to unknown environment

When the environment is unknown (i.e. there is no information on the obstacles in the room), the first step of the TL approach could not be applied as the VANs positions are unknown. To solve this problem, we can easily assume that there are measurements about another localization metric such as ToA, RSS and AoA[3]. In this case, the LoS/NLoS components of these metrics offer suitable localization accuracy. To do so, if for instance both AoA and ToA measurments are available, the rays of both metrics are sorted in a decreasing order in terms of power. The first ray will be denoted as the LoS and the rest are the NLoS rays. The receiver position will be then deduced as the intersection point which verifies both the AoA and ToA based distance equations. The algorithm for Rx localization is defined as follows.

- Find the distance between the Tx $\mathbf{p}^{Tx}$ and Rx $\mathbf{p}_1^{Rx}$ using ToA measurements of the first path. Theoretically, the distance of travel for the first ray is calculated from the ToA as follows:

$$\rho_{1,0} = c * toa_{1,0} \tag{6}$$

where c is the speed of light, $\rho_{1,0}$ is the distance traveled by the first ray (LoS ray) and $toa_{1,0}$ is the ToA of the first ray, assumed to be in LoS.
- Find $\theta'_{1,0}$, the triangulated angle of $\theta_{1,0}$ i.e. the AoA of the first ray (LoS ray), as follows:

$$\begin{cases} \theta'_{1,0} = \pi/2 - \theta_{1,0}, 0 \leq \theta_{1,0} \leq \pi/2 \\ \theta'_{1,0} = \theta_{1,0} - \pi/2, \pi/2 \leq \theta_{1,0} \leq \pi \\ \theta'_{1,0} = 3\pi/2 - \theta_{1,0}, \pi \leq \theta_{1,0} \leq 3\pi/2 \\ \theta'_{1,0} = \theta_{1,0} - 3\pi/2, 3\pi/2 \leq \theta_{1,0} \leq 2\pi \end{cases} \tag{7}$$

- Estimate the position of the receiver as follows:

$$\mathbf{P^{Rx}} = \mathbf{P^{Tx}} + \rho_{1,0} \times \mathbf{\Omega} \times \begin{bmatrix} \sin\theta'_{1,0} \\ \cos\theta'_{1,0} \end{bmatrix} \tag{8}$$

where $\mathbf{p}_1^{Rx} = \begin{bmatrix} x_1^{Rx} & y_1^{Rx} \end{bmatrix}^T$, $\mathbf{p}^{Tx} = \begin{bmatrix} x^{Tx} & y^{Tx} \end{bmatrix}^T$ and $\mathbf{\Omega}$ is defined as follows:

$$\begin{cases} \mathbf{\Omega} = \begin{bmatrix} -1 & -1 \end{bmatrix}^T, 0 \leq \theta_{1,0} \leq \pi/2 \\ \mathbf{\Omega} = \begin{bmatrix} 1 & -1 \end{bmatrix}^T, \pi/2 \leq \theta_{1,0} \leq \pi \\ \mathbf{\Omega} = \begin{bmatrix} 1 & 1 \end{bmatrix}^T, \pi \leq \theta_{1,0} \leq 3\pi/2 \\ \mathbf{\Omega} = \begin{bmatrix} -1 & 1 \end{bmatrix}^T, 3\pi/2 \leq \theta_{1,0} \leq 2\pi \end{cases} \tag{9}$$

[3]This assumption is valid as these measurements are primordial for channel estimation at mmWaves

It is very clear from these derivations that localization in mmWave can be easily done with or without environment knowledge as long as there is sufficient measurements. Moreover, it is straightforward to mention that the availability of the LoS components highly improves the accuracy of the localization approaches. In case the LoS ray is not available, the estimation of the Rx position will be biased. However, as shown in [30], the estimation error could be very small if appropriate algorithms are implemented. In this paper, we are not tackling the separation between LoS and NLoS components even though it is possible [30]. Our main focus however is to propose suitable approaches for obstacle localization and mapping keeping in mind that the accuracy of the localization approaches will enhance the accuracy of the context and environment mapping. The latter is tackled in the next section.

IV. Context Inference and Obstacle Mapping

The main target of this section is to estimate obstacles locations and their dimensions using the received signal at Rx. MOSAIC implements obstacle detection in two steps: (1) estimating the position of the VANs using TL (i.e. using AoA), RSS and TDoA; (2) estimating the obstacle direction and obstacle dimensions[4].

A. Estimation of VANs positions

Here, three different algorithms are proposed depending on the available meeasurement metrics. The first algorithm is based on the TL discussed earlier, the second one is based on the RSS while the third is based on TDoA.

1) Algorithm 1: TL for Estimating VANs: As stated above, the first step consists in estimating the positions of the VANs. However, these depend on the obstacles whose positions and dimensions are assumed unknown. Mathematically speaking, this requires estimating the different parameters $(x_{v_i}, y_{v_i}, \rho_{1,i})$ which represent the coordinates of the VANs and their distances with respect to the receiver.

The scenario is developed under harsh conditions, i.e. one transmitter and one receiver are only available for both localization and context inference. Hence, to deal with these conditions, we propose to move the receiver step-by-step while updating the estimation. Technically, the estimation of $(x_{v_i}, y_{v_i}, \rho_{1,i})$ depends on the relative position of the receiver with respect to the VANs, as shown in Fig. 3. For instance, assuming that the AoA for the LoS path between the transmitter and receiver and the AoA for the NLoS path (LoS virtually) between the transmitter and receiver (VAN and receiver) fall in the first quadrant, the system of equations describing the relation between the different parameters in $(x_{v_i}, y_{v_i}, \rho_{1,i})$ defined in (2) and (3) is as follows:

$$\begin{cases} x_{v_i} - x_{Rx} = \rho_{1,i} \times \cos\theta_{1,i} \\ x_{Rx} - x_{Tx} = \rho_{1,0} \times \sin\theta_{1,0} \end{cases} \tag{10}$$

$$\begin{cases} y_{v_i} - y_{Rx} = \rho_{1,i} \times \sin\theta_{1,i} \\ y_{Rx} - y_{Tx} = \rho_{1,0} \times \cos\theta_{1,0} \end{cases} \tag{11}$$

[4]All the calculations hereafter are presented in ideal conditions, i.e. without measurements errors, for the sake of simplification. However, in simulations, a bias due to measurements errors is added to different models

where $\rho_{1,0}$ is the distance between the original receiver position and the transmitter, $\theta_{1,0}$ is the AoA for the LoS link between the transmitter and the receiver, $\rho_{1,i}$ is the distance between the VAN to be localized and the original receiver position and $\theta_{1,i}$ is the AoA for the NLoS link corresponding to $\mathbf{v}_i$. By solving the above two systems of equations, we obtain:

$$\begin{cases} x_{v_i} - x_{Tx} = \rho_{1,0} \times \sin\theta_{1,0} + \rho_{1,i} \times \cos\theta_{1,i} \\ y_{v_i} - y_{Tx} = \rho_{1,0} \times \cos\theta_{1,0} + \rho_{1,i} \times \sin\theta_{1,i} \end{cases} \quad (12)$$

The receiver now is moved to a new position $\mathbf{p}_2^{Rx}$ as shown in Fig. 3 so that we can solve the new system of equations where the unknown variables become the positions of the VANs. The same procedure is repeated over a new AoA spectrum corresponding to the new receiver position.
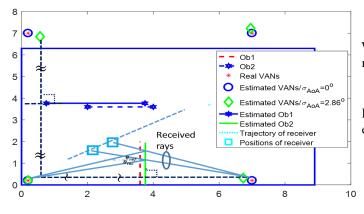

Fig. 3. Estimated VANs by moving the receiver from $\mathbf{p}_1^{Rx}$ to $\mathbf{p}_2^{Rx}$

The new system of equations defines the relation between the parameters in $(x_{v_i}, y_{v_i}, \rho_{1,i})$ corresponding to the new receiver position is given by:

$$\begin{cases} x_{v_i} - x_{Tx} = \rho_{2,0} \times \sin\theta_{2,0} + \rho_{2,i} \times \cos\theta_{2,i} \\ y_{v_i} - y_{Tx} = \rho_{2,0} \times \cos\theta_{2,0} + \rho_{2,i} \times \sin\theta_{2,i} \end{cases} \quad (13)$$

where $\rho_{2,i}$ and $\theta_{2,i}$ are the distance and the AoA, respectively, corresponding to the link between the VAN $\mathbf{v}_i$ and the new receiver position $\mathbf{p}_2^{Rx}$. Then, the estimation of the VANs is done by combining the two systems of equations in (12) and (13). This leads to the following:

$$\begin{bmatrix} \cos\theta_{1,i} & -\cos\theta_{2,i} \\ \sin\theta_{1,i} & -\sin\theta_{2,i} \end{bmatrix} \begin{bmatrix} \rho_{1,i} \\ \rho_{2,i} \end{bmatrix} = \begin{bmatrix} -\sin\theta_{1,0} & \sin\theta_{2,0} \\ -\cos\theta_{1,0} & \cos\theta_{2,0} \end{bmatrix} \begin{bmatrix} \rho_{1,0} \\ \rho_{2,0} \end{bmatrix} \quad (14)$$

The two unknowns, $\rho_{1,i}$ and $\rho_{2,i}$, are calculated as follows:

$$\begin{bmatrix} \rho_{1,i} \\ \rho_{2,i} \end{bmatrix} = \Sigma^{-1} \begin{bmatrix} -\sin\theta_{1,0} & \sin\theta_{2,0} \\ -\cos\theta_{1,0} & \cos\theta_{2,0} \end{bmatrix} \begin{bmatrix} \rho_{1,0} \\ \rho_{2,0} \end{bmatrix} \quad (15)$$

where $\Sigma = \begin{bmatrix} \cos\theta_{1,i} & -\cos\theta_{2,i} \\ \sin\theta_{1,i} & -\sin\theta_{2,i} \end{bmatrix}$. $\rho_{1,i}$ and $\rho_{2,i}$ are then replaced in (12) or (13) to estimate x_{v_i} and y_{v_i}. Knowing that RRCs come from the transmitter via a LoS link and from VANs via NLoS links, this process is iterated over all entries of the AoA power spectrum $SP_{\mathbf{p}}(\theta)$, a $(2 \times N_p)$ matrix, to estimate the positions of all VANs. The calculations are repeated at every receiver position.

2) Algorithm 2: RSS for Estimating VANs: The RSS approach can be also used to estimate the positions of VANs required for obstacle detection. The received power at these anchor nodes follows a log-normal shadowing pathloss model in mmwave channels [31][32]. The received power, P_i, is calculated using the following equation:

$$P_i[dBm] = P_0 - 10\eta \log_{10}\rho_i + w_i, i = 1, \ldots, N_p - 1 \quad (16)$$

where P_0 is the power at the reference distance ρ_0, η is the pathloss exponent (PLE), ρ_i is the Euclidean distance between the receiver and the VAN $\mathbf{v}_i$, N_p is the number of RRCs, and w_i is the zero mean Gaussian random variable measured in dB scale with shadowing fading effect described by the standard deviation σ_{RSS}. The square of the distance ρ_i between the VAN $\mathbf{v}_i$ and the receiver $\mathbf{p}^{Rx}$ is represented as follows:

$$\rho_i^2 = \left\| \mathbf{v}_i - \mathbf{p}^{Rx} \right\|_2^2 = \left(x_{v_i} - x^{Rx} \right)^2 + \left(y_{v_i} - y^{Rx} \right)^2 \quad (17)$$

Without loss of generality, we assume the transmitter to be the reference. Hence, for $i >= 1$, we define the following:

$$x^{Rx}\rho_i^2 - \rho_0^2 = x_{v_i}^2 - 2x^{Rx}x_{v_i} + y_{v_i}^2 - 2y^{Rx}y_{v_i} \quad (18)$$

Expressing (18) in matrix form, we obtain the following equation:

$$\begin{bmatrix} 2x_1 & 2y_1 \\ \vdots & \vdots \\ 2x_{N_p-1} & 2y_{N_p-1} \end{bmatrix} \cdot \begin{bmatrix} x^{Rx} \\ y^{Rx} \end{bmatrix} = \\ \begin{bmatrix} x_1^2 - x_0^2 + y_1^2 - y_0^2 + \rho_0^2 - \rho_1^2 \\ \vdots \\ x_{N_p-1}^2 - x_0^2 + y_{N_p-1}^2 - y_0^2 + \rho_0^2 - \rho_{N_p-1}^2 \end{bmatrix} \quad (19)$$

The real distance ρ_i is not known in RSS localization; hence, noisy estimations of the distance, $\tilde{\rho}_i$, obtain from (16), are related with the unknown position of the receiver $\mathbf{p}^{Rx} = \begin{bmatrix} x^{Rx}, y^{Rx} \end{bmatrix}^T$ as follows:

$$\mathbf{R}\mathbf{p}^{Rx} = \mathbf{T} \quad (20)$$

where $\mathbf{R}$ and $\mathbf{T}$ are defined as follows:

$$\mathbf{R} = \begin{bmatrix} 2(x_1 - x_0) & 2(y_1 - y_0) \\ \vdots & \vdots \\ 2(x_{N_p-1} - x_0) & 2(y_{N_p-1} - y_0) \end{bmatrix}$$

$$\mathbf{T} = \begin{bmatrix} x_1^2 - x_0^2 + y_1^2 - y_0^2 + \rho_0^2 - \rho_1^2 \\ \vdots \\ x_{N_p-1}^2 - x_0^2 + y_{N_p-1}^2 - y_0^2 + \rho_0^2 - \rho_{N_p-1}^2 \end{bmatrix}$$

Here, we write directly the system of equations at N different positions $\left\{ \mathbf{p}_1^{Rx}, \mathbf{p}_2^{Rx}, \ldots, \mathbf{p}_N^{Rx} \right\}$. Hence, the following system of equations is generated based on the difference between the measurements taken at $\mathbf{p}_1^{Rx}$ and $\mathbf{p}_n^{Rx}$, $n = 2, \ldots N^{Rx}$, respectively:

$$\mathbf{R} \left(\mathbf{p}_1^{Rx} - \mathbf{p}_n^{Rx} \right) = \mathbf{T}_1 - \mathbf{T}_n$$

$$= \begin{bmatrix} \tilde{\rho}_{0/Rx1}^2 - \tilde{\rho}_{1/Rx1}^2 - \tilde{\rho}_{0/Rxn}^2 + \tilde{\rho}_{1/Rxn}^2 \\ \vdots \\ \tilde{\rho}_{0/Rx1}^2 - \tilde{\rho}_{N_p-1/Rx1}^2 - \tilde{\rho}_{0/Rxn}^2 + \tilde{\rho}_{N_p-1/Rxn}^2 \end{bmatrix} \quad (21)$$

where $\tilde{\rho}_{i/Rxn}^2$ is the estimated distance between VAN $\mathbf{v}_i$ and the receiver at position $\mathbf{p}_n^{Rx}$, knowing that $\rho_{i/Rxn}^2$ is defined as follows:

$$\rho_{i/Rxn}^2 = \left\| \mathbf{v}_i - \mathbf{p}_n^{Rx} \right\|_2^2 = \left(x_{v_i} - x_{p_n^{Rx}} \right)^2 + \left(y_{v_i} - y_{p_n^{Rx}} \right)^2 \qquad (22)$$

The target is to estimate $\mathbf{R}$ in order to estimate the positions of the VANs. A simple Least Square (LS) estimator gives:

$$\hat{\mathbf{R}} = \mathbf{T}_d \cdot \mathbf{P}_d^T \left(\mathbf{P}_d \mathbf{P}_d^T \right)^{-1} \qquad (23)$$

where $\mathbf{T}_d$ and $\mathbf{P}_d$ are now defined as follows:

$$\mathbf{P}_d = \left[\begin{array}{cccc} \mathbf{p}_1^{Rx} - \mathbf{p}_2^{Rx} & \mathbf{p}_1^{Rx} - \mathbf{p}_3^{Rx} & \dots & \mathbf{p}_1^{Rx} - \mathbf{p}_{N_{Rx}}^{Rx} \end{array} \right] \qquad (24)$$

$$\mathbf{T}_d = \left[\begin{array}{cccc} \mathbf{T}_1 - \mathbf{T}_2 & \mathbf{T}_1 - \mathbf{T}_3 & \dots & \mathbf{T}_1 - \mathbf{T}_{N_{Rx}} \end{array} \right] \qquad (25)$$

As a result, the positions of the VANs are estimated as follows:

$$\left[\begin{array}{cc} x_1 & y_1 \\ \vdots & \vdots \\ x_{N_p-1} & y_{N_p-1} \end{array} \right] = \frac{1}{2}\hat{\mathbf{R}} + \left[\begin{array}{cc} x_0 & y_0 \\ \vdots & \vdots \\ x_0 & y_0 \end{array} \right] \qquad (26)$$

3) Algorithm 3: TDoA for Estimating VANs: TDoA can be also used for the estimation of the VANs. The distances between the receiver and the VAN $\mathbf{v}_i$ in absence of noise is represented as follows:

$$\rho_0^i = c \times t_0^i = \rho_i - \rho_0, \quad i = 1, \dots, N_p - 1 \qquad (27)$$

where t_0^i is the TDoA of the received signal at the pair of the VAN $\mathbf{v}_i$ and the transmitter respectively, and c is the speed of the signal propagation. As shown in (27), the estimated TDoAs are converted to range difference of arrival (RDoA) measurements creating a set of nonlinear equations describing the hyperbolic range difference. The receiver position can be estimated from the intersection of the resultant hyperboloids. In realistic scenarios, RDoA measurements $\tilde{\rho}_0^i$ are obtained with noise as modeled in the following equation:

$$\tilde{\rho}_0^i = \rho_0^i + w_0^i = \rho_i - \rho_0 + w_0^i, \quad i = 1, \dots, N_p - 1 \qquad (28)$$

where w_{i1} is the zero mean Gaussian random noise vector of the RDoA measurement. (28) can be written as $\tilde{\rho}_0^i + \rho_0 = \rho_i + w_0^i$. Hence, squaring and substituting with (17), we obtain:

$$x^{Rx}(x_i - x_0) + y^{Rx}(y_i - y_0) + \rho_0 \tilde{\rho}_0^i =$$
$$\frac{1}{2}\left[\left(x_i^2 - x_0^2 \right) + \left(y_i^2 - y_0^2 \right) - \tilde{\rho}_0^{i\,2} \right] + \frac{1}{2}\,w_0^{i\,2} + \rho_i w_0^i \qquad (29)$$

Hence, the model is given by:

$$\mathbf{G} \cdot \mathbf{p}^{Rx} = \mathbf{H} \qquad (30)$$

where $\mathbf{G}$, and $\mathbf{H}$ are defined as follows:

$$\mathbf{G} = \left[\begin{array}{cc} x_1 - x_0 & y_1 - y_0 \\ \vdots & \vdots \\ x_{N_p-1} - x_0 & y_{N_p-1} - y_0 \end{array} \right]$$

$$\mathbf{H} = \left[\begin{array}{c} \frac{1}{2}\left(m_0^1 - \tilde{\rho}_0^{1\,2} \right) - \rho_0 \tilde{\rho}_0^1 \\ \vdots \\ \frac{1}{2}\left(m_0^{N_p-1} - \tilde{\rho}_0^{N_p-1\,2} \right) - \rho_0 \tilde{\rho}_0^{N_p-1} \end{array} \right]$$

where $m_0^i = \mathbf{v}_i^T \mathbf{v}_i - \mathbf{p}^{Tx\,T} \mathbf{p}^{Tx}$. Knowing that the measurement error w_0^i is small, the noise vector ϵ_0 is approximated as follows:

$$\epsilon_0 \approx \left[w_0^1 \rho_1, \dots, w_0^{N_p-1} \rho_{N_p-1} \right]^T \qquad (31)$$

Three TDoA measurements are observed at three different positions of the receiver $\mathbf{p}_1^{Rx}$, $\mathbf{p}_2^{Rx}$ and $\mathbf{p}_3^{Rx}$ respectively. The following system of equations is constructed based on the difference between the measurements taken at $\mathbf{p}_1^{Rx}$ and $\mathbf{p}_2^{Rx}$ and those taken at $\mathbf{p}_1^{Rx}$ and $\mathbf{p}_3^{Rx}$, respectively:

$$\mathbf{G}\left(\mathbf{p}_1^{Rx} - \mathbf{p}_2^{Rx} \right) = \mathbf{H}_1 - \mathbf{H}_2$$
$$= \left[\begin{array}{c} \frac{1}{2}\left(\tilde{\rho}_{0/Rx2}^{1\,2} - \tilde{\rho}_{0/Rx1}^{1\,2} \right) + \rho_{0/Rx2}\tilde{\rho}_{0/Rx2}^1 - \rho_{0/Rx1}\tilde{\rho}_{0/Rx1}^1 \\ \vdots \\ \frac{1}{2}\left(\tilde{\rho}_{0/Rx2}^{N_p-1\,2} - \tilde{\rho}_{0/Rx1}^{N_p-1\,2} \right) + \rho_{0/Rx2}\tilde{\rho}_{0/Rx2}^{N_p-1} - \rho_{0/Rx1}\tilde{\rho}_{0/Rx1}^{N_p-1} \end{array} \right] \qquad (32)$$

$$\mathbf{G}\left(\mathbf{p}_1^{Rx} - \mathbf{p}_3^{Rx} \right) = \mathbf{H}_1 - \mathbf{H}_3$$
$$= \left[\begin{array}{c} \frac{1}{2}\left(\tilde{\rho}_{0/Rx3}^{1\,2} - \tilde{\rho}_{0/Rx1}^{1\,2} \right) + \rho_{0/Rx3}\tilde{\rho}_{0/Rx3}^1 - \rho_{0/Rx1}\tilde{\rho}_{0/Rx1}^1 \\ \vdots \\ \frac{1}{2}\left(\tilde{\rho}_{0/Rx3}^{N_p-1\,2} - \tilde{\rho}_{0/Rx1}^{N_p-1\,2} \right) + \rho_{0/Rx3}\tilde{\rho}_{0/Rx3}^{N_p-1} - \rho_{0/Rx1}\tilde{\rho}_{0/Rx1}^{N_p-1} \end{array} \right] \qquad (33)$$

Equations (32) and (33) can be written in matrix notations as:

$$\mathbf{G} \cdot \mathbf{P}_d = \mathbf{H}_d \qquad (34)$$

where $\mathbf{P}_d$ and $\mathbf{H}_d$ are defined as follows:

$$\mathbf{P}_d = \left[\begin{array}{cc} \mathbf{p}_1^{Rx} - \mathbf{p}_2^{Rx} & \mathbf{p}_1^{Rx} - \mathbf{p}_3^{Rx} \end{array} \right] \qquad (35)$$

$$\mathbf{H}_d = \left[\begin{array}{cc} \mathbf{H}_1 - \mathbf{H}_2 & \mathbf{H}_1 - \mathbf{H}_3 \end{array} \right] \qquad (36)$$

The LS solution of $\mathbf{G}$ yields:

$$\hat{\mathbf{G}} = \mathbf{H}_d \cdot \mathbf{P}_d^{-1} \qquad (37)$$

As a result, the positions of the VANs are estimated as follows:

$$\left[\begin{array}{cc} x_1 & y_1 \\ \vdots & \vdots \\ x_{N_p-1} & y_{N_p-1} \end{array} \right] = \hat{\mathbf{G}} + \left[\begin{array}{cc} x_0 & y_0 \\ \vdots & \vdots \\ x_0 & y_0 \end{array} \right] \qquad (38)$$

It is worth mentioning that all these solutions could be easily updated to Weighted LS (WLS) or other estimators. Therein, we restrict ourself to the WLS solution for the RSS given in Appendix due to lack of space.

B. Obstacle Detection

After the estimation of the VANs, the target is to detect the obstacles in the room. Referring to Fig. 3, obstacle detection is achieved using either RSS and AoA or TDoA and AoA. The obstacle detection is done by the following steps:

- The VANs positions are firstly estimated as detailed in the previous section.
- Since the VANs are the mirrors of the transmitter with respect to all surfaces of the obstacles in the room, the obstacles are then the perpendicular to the line connecting the transmitter to each estimated VAN respectively. The perpendicular line passes through the midpoint of the segment $\left[\mathbf{v}_i \mathbf{p}^{Tx} \right]$.
- Equation (1) is used to write the equation of the obstacle surface, where α and $\mathbf{p} = \left[p_x, p_y \right]$ are the slope and

midpoint of segment $\left[\mathbf{v}_i \mathbf{p}^{Tx}\right]$, respectively. Fig. 3 shows the estimated obstacles by firstly estimating its location (the midpoint between Tx and VAN) and direction.

- Using the AoA and the estimated positions of the receiver, VAN and obstacle, the point of reflection at the obstacle can be easily deduced. It is simply the point of intersection between the line $\left[\mathbf{v}_i, \mathbf{p}^{Rx}\right]$ and the obstacle line. Definitely, this point of reflection is a point on the obstacle.
- At each receiver measurement, this procedure is iterated over all pairs of $\left(\mathbf{v}_i, \mathbf{p}^{Tx}\right), i = 1, 2, \ldots, N_p$, where N_p is the number of VANs. At each iteration, an estimated point of reflection belonging to the obstacle side is created. Using all these measurements, a cloud (set) of reflection points (CoRP) is generated.
- Using the CoRP, an interpolation between these points is applied. It is followed by a simple smoothing operation.

In summary, obstacle surfaces are detected and estimated using a set of connected reflection points. Using the concept of mirroring, we iterate over all pairs of $\left(\mathbf{v}_i, \mathbf{p}^{Tx}\right)$ to detect an obstacle surface. Then, the problem turns down to estimate the obstacle limits.

C. Obstacle Dimensioning: Finding the Obstacle Limits
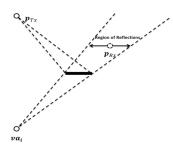

Fig. 4. Region of possible reflections

After detecting the direction of the obstacles in the room and its corresponding position, the boundaries of the obstacle are left to be set. Here two approaches could be applied (jointly or separately):

Approach 1: Estimate the vertices by power measurements As shown in Fig. 4, a point of reflection is obtained at the obstacle if the receiver moves within the region of all possible reflections determined by the obstacle limits, the position of the transmitter, and the related VAN. Hence, the AoA/TDoA/RSS spectrum generated at all receiver positions will dramatically change when the receiver leaves the region of reflection. Indeed, mmWave signals suffer from absorption loss by each obstacle. Hence, a change in the reflection environment will change. Without loss of generality, when the receiver moves to the right or to the left outside the region of reflection shown in Figure 4, the power of the received signal at the corresponding AoA will dramatically change raising the existence of the object limit. So the latter could be estimated by a simple border detection through power measurements, i.e separating the power of an obstacle ray from noise or walls rays. In this paper, the detection is based on a simple energy detector algorithm whose threshold is set to maximize the

probability of detection.

Approach 2: Estimate the vertices as intersections of the obstacle sides: This approach could be applied if the obstacle is of 2D shape (not 1D). As shown in the previous section, each side of the obstacle is firstly determined via its direction and a point on it. Hence, the limits (i.e. the vertices) of the obstacles are simply determined by the intersections of these sides.

D. Clustering the Cloud of Vertices Points

Each measurement at each Rx position provides an estimation of the point of reflection first and then, through obstacle limits calculations, provides an estimation of the vertices constituting the obstacle. However, as these measurements are biased due to noise, a clustering of all measurements is required. Without loss of generality, the K-means algorithm [33] has been used to cluster the set of estimates of the obstacle vertices. Then, the sum of absolute differences approach is implemented to specify the centroids of the clusters. The latter represent the component-wise median of a set of estimations for an obstacle vertex.

E. Discussion on MOSAIC

One AN was used so far for receiver localization and obstacle detection. If the obstacle is known then the estimation of the receiver position follows from the VANs positions. However, when the obstacle information is not available, the estimation of both the receiver and the VANs positions can be done if enough measurements metrics (TDoA and AoA, RSS and AoA) are available.

The estimation accuracy depends on the availability of LoS path. When it is not available, the measurements (mainly the AoA) will be biased since in our approach, the first path is considered to be the LoS. To overcome this problem and reduce the bias, it is very important to increase the number of ANs leading to an increase in the LoS measurements. This is indeed one of the major problems in mmWave systems. On the other side, the limits of the obstacle are estimated if and only if the receiver is within the range of reflection. Nevertheless, this is not always the case with a single receiver at a given position and single AN. Consequently, at a receiver position, increasing the number of ANs will also enhance the estimation accuracy of the obstacle limits. So, a question arises: how many ANs do we need in MOSAIC?

V. Optimal Number of ANs

The target in this section is to explore the effect of increasing the number of ANs in terms of localization accuracy and mapping capabilities. Indeed, it has been shown in the previous section that the environment mapping depends on the estimation of the VANs which depends on the localization accuracy of the receiver. However, increasing the number of ANs indefinitely leads to additional measurements to be processed from one side and might not provide the best accuracy from the other side. To answer this question, we derive the CRLB of each algorithm proposed in Section 4 at each position of the Rx.

A. CRLB Derivations with N ANs

The optimal number of ANs needed is analyzed via CRLB optimization for each metric.

1) CRLB for Algorithm 1 (The TL Approach): Here, we assume that the AoA measurements taken at the receiver coming from all ANs are independent. Assuming a wideband multipath model, we estimate the receiver position using the TL and ADoA techniques based on a Gaussian AoA model. This model represents scenarios where there is a strong LoS component that could be resolved by the receiver separately from multiple NLoS components due to local scattering. For a single transmitter $\mathbf{p}^{Tx}$ with an AoA $\theta(\mathbf{p}^{Tx})$ at the receiver, we consider a Gaussian LoS model with local scattering defined as:

$$p_{LoS}\left(\hat{\theta}/\mathbf{p}^{Tx}\right) = \frac{1}{\sqrt{2\pi}\sigma\left(1 - 2Q\left(\frac{\pi}{2\sigma}\right)\right)}\exp(-\frac{\left(\hat{\theta} - \theta\left(\mathbf{p}^{Tx}\right)\right)^2}{2\sigma^2} \quad (39)$$

where $\hat{\theta} \in [0, \pi]$, $Q(t) = \int_t^\infty \exp(-t^2/2)/\sqrt{2\pi}dt$ and σ^2 is the estimation error variance, representing the spatial extent of scattering. Additionally, the remaining AoA measurements due to reflected and scattered NLoS paths are assumed to be virtually in LoS with VANs. Hence, the distribution of these NLoS paths is defined as follows:

$$p_{NLoS}\left(\hat{\theta}_i/\mathbf{v}_i\right) = \frac{1}{\sqrt{2\pi}\sigma\left(1 - 2Q\left(\frac{\pi}{2\sigma}\right)\right)}\exp(-\frac{\left(\hat{\theta}_i - \theta_i\left(\mathbf{v}_i\right)\right)^2}{2\sigma^2} \quad (40)$$

where $\theta_i(\mathbf{v}_i)$ is the true AoA coming from the VAN $\mathbf{v}_i$ to the receiver knowing that $\mathbf{v}_0 = \mathbf{p}^{Tx}$. Hence, the AoA estimates are generated for a wideband multipath model based on the following distribution:

$$p_{wideband}\left(\hat{\theta}_1, \hat{\theta}_2, \ldots, \hat{\theta}_{N_p}/\mathbf{p}^{Tx}\right) = p_{LoS}\left(\hat{\theta}_1/\mathbf{p}^{Tx}\right)p_{NLoS}\left(\hat{\theta}_2/\mathbf{v}_2\right)\ldots p_{NLoS}\left(\hat{\theta}_{N_p}/\mathbf{v}_{N_p}\right) \quad (41)$$

where N_p is the number of RRCs. Accordingly, the log-likelihood function for the estimates of the AoA for all RRCs is as follows:

$$L\left(\hat{\theta}_1, \hat{\theta}_2, \ldots, \hat{\theta}_{N_p}/\mathbf{p}^{Tx}, V\right) = -\sum_{i=0}^{N_p}\frac{\left(\hat{\theta}_i - \theta_i\left(\mathbf{v}_i\right)\right)^2}{\sigma^2} \quad (42)$$

Based on what has been derived for single transmitter in terms of the probability density function (pdf) of the wideband multipath model in (41), the log-likelihood function for the estimates of the AoA for all RRCs corresponding to multiple transmitters is as follows:

$$L\left(\hat{\theta}_1, \hat{\theta}_2, \ldots, \hat{\theta}_{N_p}/\mathbf{p}^{Tx}, V\right) = -\sum_{m=1}^{N_{Tx}}\sum_{i=0}^{N_p}\frac{\left(\hat{\theta}_i - \theta_i\left(\mathbf{v}_{m,i}\right)\right)^2}{\sigma^2} \quad (43)$$

where $\theta_i(\mathbf{v}_{m,i})$ is the true AoA coming from the VAN $\mathbf{v}_{m,i}$ corresponding to the transmitter $\mathbf{p}_m^{Tx}$ reaching the receiver $\mathbf{p}^{Rx}$ and $\mathbf{v}_{m,0} = \mathbf{p}_m^{Tx}$. Then, we construct the Fisher information matrix (FIM) $\mathbf{F}\left(\left\{\mathbf{p}^{Tx}, V\right\}\right)$ in order to calculate the CRLB, which is $\mathbf{F}^{-1}\left(\left\{\mathbf{p}^{Tx}, V\right\}\right)$. For the Gaussian model in (41), $\mathbf{F}\left(\left\{\mathbf{p}^{Tx}, V\right\}\right)$ is defined as follows:

$$F\left(\{\mathbf{p}_{Tx}, V\}\right) =$$
$$\begin{pmatrix} \sum_{m=1}^{N_{Tx}}\sum_{i=0}^{N_p}\frac{\sin^2(\theta_i)}{\sigma^2\rho_{m,i}^2} & -\sum_{m=1}^{N_{Tx}}\sum_{i=0}^{N_p}\frac{\cos(\theta_i)\sin(\theta_i)}{\sigma^2\rho_{m,i}^2} \\ -\sum_{m=1}^{N_{Tx}}\sum_{i=0}^{N_p}\frac{\cos(\theta_i)\sin(\theta_i)}{\sigma^2\rho_{m,i}^2} & \sum_{m=1}^{N_{Tx}}\sum_{i=0}^{N_p}\frac{\cos^2(\theta_i)}{\sigma^2\rho_{m,i}^2} \end{pmatrix} \quad (44)$$

where $\rho_{m,i}$ is the distance between $\mathbf{v}_{m,i}$ corresponding to the transmitter $\mathbf{p}_m^{Tx}$ and the receiver $\mathbf{p}^{Rx}$. Knowing that the total error of localizing the receiver is the sum of variances along x and y, we define the CRLB for localization under NLoS environment using the TL technique as follows:

$$CRLB_{AOA|NLoS} = Tr\left(\mathbf{F}^{-1}\left(\left\{\mathbf{p}^{Tx}, V\right\}\right)\right)$$
$$= \frac{\sigma^2\sum_{m=1}^{N_{Tx}}\sum_{i=0}^{N_p}\frac{1}{\rho_{m,i}^2}}{\sum_{m=1}^{N_{Tx}}\sum_{i=0}^{N_p}\sum_{k=i+1}^{N_p}\frac{\sin^2(\theta_i - \theta_k)}{\rho_{m,i}^2\rho_{m,k}^2}} \quad (45)$$

In case of LoS environment, the CRLB for localization using TL technique based on AoA approach is as follows:

$$CRLB_{AOA|LoS} = \frac{\sigma^2\sum_{m=1}^{N_{Tx}}\frac{1}{\rho_{m,LoS}^2}}{\sum_{m=1}^{N_{Tx}}\sum_{k=m+1}^{N_{Tx}}\frac{\sin^2(\theta_m - \theta_k)}{\rho_{m,LoS}^2\rho_{k,LoS}^2}} \quad (46)$$

2) CRLB for Algorithm 2 (RSS Metric): : In RSS based approach, the log likelihood function (LLF) of the pdf of P_i is expressed as follows:

$$\log\left(Pr\left(\mathbf{P}; \mathbf{d}\right)\right) =$$
$$\log\left[\prod_{m=1}^{N_{Tx}}\prod_{i=1}^{N_p}\frac{10/\log 10}{\sqrt{2\pi\sigma_{RSS}^2}}\frac{1}{P_{m,i}}\exp\left[-\frac{\left(\frac{10\eta}{\sigma_{RSS}\log 10}\right)^2}{8}\left(\log\frac{d_{m,i}^2}{\tilde{d}_{m,i}^2}\right)^2\right]\right]$$
$$= N_{Tx} \times N_p \times \log\left(\frac{10}{\log(10)\sqrt{2\pi\sigma_{RSS}^2}}\right) + \quad (47)$$
$$\sum_{m=1}^{N_{Tx}}\sum_{i=1}^{N_p}\left(\log\left(\frac{1}{P_{m,i}}\right) - \frac{\left(\frac{10\eta}{\sigma_{RSS}\log 10}\right)^2}{2}\left(\log\left(\frac{d_{m,i}}{\tilde{d}_{m,i}}\right)\right)^2\right)$$

where $d_{m,i}$ is the distance between the VAN $\mathbf{v}_{m,i}$ corresponding to the transmitter $\mathbf{p}_m^{Tx}$ and the receiver $\mathbf{p}^{Rx}$ and $\tilde{d}_{m,i}$ is its estimate. Then, the second partial derivative is defined as follows:

$$\frac{\partial^2\left(\log\left(Pr\left(\mathbf{P}; \mathbf{d}\right)\right)\right)}{\partial\mathbf{d}^2} = -\frac{\left(\frac{10\eta}{\sigma_{RSS}\log 10}\right)^2}{\ln 10}\sum_{m=1}^{N_{Tx}}\sum_{i=1}^{N_p}\frac{1}{d_{m,i}^2}\left(\frac{1}{\ln 10} - \log\left(\frac{d_{m,i}}{\tilde{d}_{m,i}}\right)\right) \quad (48)$$

Hence, the optimal number of ANs is obtained by optimizing the following CRLB for a target localization accuracy:

$$CRLB_{RSS} = \frac{-1}{\frac{\partial^2\left(\log(Pr(\mathbf{P}; \mathbf{d}))\right)}{\partial\mathbf{d}^2}}$$
$$= \frac{\ln 10}{\left(\frac{10\eta}{\sigma_{RSS}\log 10}\right)^2}\frac{1}{\sum_{m=1}^{N_{Tx}}\sum_{i=1}^{N_p}\frac{1}{d_{m,i}^2}\left(\frac{1}{\ln 10} - \log\left(\frac{d_{m,i}}{\tilde{d}_{m,i}}\right)\right)} \quad (49)$$

3) CRLB for Algorithm 3 (TDoA Metric): The ToA measurements taken at the receiver from multiple ANs are assumed to be independent. The distances between the receiver and the VAN $\mathbf{v}_{m,i}$ corresponding to the transmitter $\mathbf{p}_m^{Tx}$ in absence of noise is represented as follows:

$$d_{m,i1} = c \times t_{m,i1} = d_{mi} - d_{m1}, m = 1, \ldots, N_{Tx} and i = 1, \ldots, N_p \quad (50)$$

where $t_{m,i1}$ is the TDoA of the received signal at the pair of the VAN $\mathbf{v}_{m,i}$ and the transmitter $\mathbf{p}_m^{Tx}$ respectively, and c is the speed of light. As shown in (50), the estimated TDoAs are converted to range difference of arrival (RDoA) measurements

creating a set of nonlinear equations describing the hyperbolic range difference. In realistic scenarios, RDoA measurements $\tilde{d}_{m,i1}$ are obtained with noise and modeled as:

$$\tilde{d}_{m,i1} = d_{m,i1} + w_{m1} = d_{mi} - d_{m1} + w_{m,i1}, m = 1, \ldots, N_{Tx} \quad (51)$$

where $i = 1, \ldots, N_p$ and $w_{m,i1}$ is the zero mean Gaussian random noise vector of the RDoA measurement with a $\left(N_p - 1\right) \times \left(N_p - 1\right)$ covariance matrix $\mathbf{\Sigma}_d$. Thus, the pdf of $\tilde{d}_{m,i1}$ defined in (51) is as follows:

$$Pr\left(\tilde{\mathbf{d}}; \mathbf{d}\right) = \prod_{m=1}^{N_{Tx}} \prod_{i=1}^{N_p} \frac{1}{\sqrt{2\pi c^2 \sigma_T^2}} \exp\left[-\frac{\left(\tilde{d}_{m,i1} - d_{m,i1}\right)^2}{2c^2\sigma_T^2}\right]$$

$$= \frac{1}{\left(2\pi c^2 \sigma_T^2\right)^{\frac{N_{Tx} \times N_p}{2}}} \exp\left[-\frac{\sum_{m=1}^{N_{Tx}} \sum_{i=1}^{N_p} \left(\tilde{d}_{m,i1} - d_{m,i1}\right)^2}{2c^2\sigma_T^2}\right] \quad (52)$$

Applying the same methodology used for RSS, we calculate the second partial derivative of the LLF for the pdf defined in (52) as follows:

$$\frac{\partial^2 \left(\log\left(Pr\left(\tilde{\mathbf{d}}; \mathbf{d}\right)\right)\right)}{\partial \mathbf{d}^2} = -\frac{N_{Tx} \times N_p}{c^2 \sigma_T^2} \quad (53)$$

Consequently, the optimal number of ANs required to achieve a TDoA localization accuracy defined by the CRLB is as follows:

$$N^*_{Tx|optimal} = \frac{c^2 \sigma_T^2}{N_p \times CRLB_{TDoA}} \quad (54)$$

B. Discussion

The CRLB of the different metrics decreases with the number of ANs, except for AoA, in which a further discussion should be provided. Indeed, when the AoA metric is used for localization and mapping, it is very important to separate between the LoS and NLoS cases. In the former, an additional number of ANs increases the resolvability of the Rx location as it will be shown in next section. However, in the case of NLoS, the increase in the ANs will increase the number of ambiguities hence it deteriorates the estimation. This is not the case in RSS or ToA since they are used to support the TL approach. Another conclusion can be derived from the calculations of the CRLBs. Equations (49) and (54) show that the number N_{Tx} of ANs and the number N_p of RRCs can be exchanged without changing in the CRLB. This means that both RSS and TDoA present similar results if the number of anchor nodes is increased or the number of reflections is increased.

Finally, the RSS measurements are sensitive to the absorption loss at mmWaves: a parameter which creates a bias in the distance estimation if it is not taken into account. In practice, the absorption loss depends on the reflection coefficient at the obstacle; it is left for future research directions.

VI. SIMULATION RESULTS

A. Parameters and Environment Settings

The room geometry is of rectangular shape of size $10 \times 10m^2$. The south-western corner of the room is assumed to be the reference of the Cartesian coordinate system. The angles

are measured with respect to the positive part of the x-axis. The transmitter is set at position $\mathbf{p}^{Tx} = (0.2, 0.2)$ m. The antenna at the transmitter is assumed to be omnidirectional; hence, the transmitted power $P_{Tx}(\theta)$ is constant for all θ. An antenna array is considered at the receiver with a reception beam pattern described as $P_{Rx}(\theta) = \exp\left(-\frac{\theta^2}{2s^2}\right)$, $s = 0.1$. The value of parameter s and the Gaussian shape have been devised empirically. Additionally, all results are simulated for 10000 realizations.

B. Performance of the Rx Localization Algorithm in unknown Environment

In this section, we provide the simulation results of the localization accuracy in an unknown environment. We remind the reader that an unknown environment refers to the case where there is no information about the obstacles in the room.
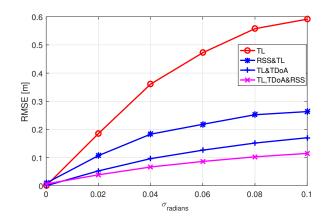

Fig. 5. Simulation Results of the Hybrid Approach

We implemented different combinations of the basic standalone positioning techniques (TL, RSS, and TDoA) to achieve additional enhancement in the localization accuracy. Fig. 5 shows the RMSE of estimating the receiver's position using TL, TL in combination with TDoA, TL in combination with RSS and TL in combination with RSS and TDoA. It is very clear that the hybrid approach presents the best results. Particularly, the combination of the TL and TDoA has a good accuracy and presents comparable results with those obtained with all metrics. In terms of localizing VANs, Fig. 6 shows that the estimation error ranges from 0 m to almost 1.9 m as the noise of the TDoA measurements σ_{TDOA} increases to 0.2 ns, depending on the number of Rx positions taken into account in the measurement process. It is clear that the accuracy of localizing the VANs presents negligible error if the number of Rx positions is increased. For instance, the error is shown to be less than 0.075 m at $\sigma_{TDOA} = 0.2$ ns and less than 0.04 m at $\sigma_{TDOA} = 0.1$ ns with 100 Rx positions. This means that a mobile receiver can perfectly estimate the positions of the VANs.
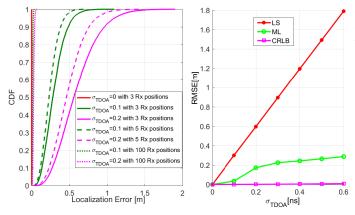
Fig. 6. Estimation error of localizing VANs based on TDoA approach using LS and ML versus σ_{TDOA}

C. Optimal Number of ANs

Increasing the number of ANs is proposed for the sake of enhancing localization and obstacle mapping accuracy. This increase is expected to increase the probability of LoS links and the number of estimations for the obstacle vertices. Thus, the optimal number of ANs is recognized as a compromise between the number that achieves the best localization accuracy and the number that achieves full detection of an obstacle. As shown in Fig. 7, the localization accuracy for TL becomes worse with the increase in the number of ANs. The decrease of the CRLB level using TL with the increase in the number of ANs is due to the NLoS environment. The AoA localization based technique is highly sensitive to errors under NLoS scenario since the rays coming from NLoS paths will deteriorate the localization accuracy. This is indeed expected as AoA is very sensitive to errors as shown in literature. For instance, an error of 5° might lead to high direction error which is translated by high position error.
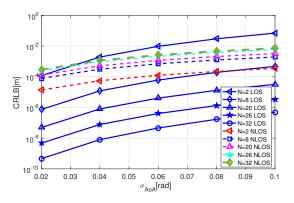

Fig. 7. CRLB of localization accuracy using AoA under LoS/NLoS conditions for various number of ANs

However, in LoS conditions, the increase in the number of ANs decreases the CRLB level of the localization accuracy as shown in Fig. 7. In such scenario, the AoA of the LoS ray is less biased to error compared to that of the NLoS ray; hence, the increase in the number of ANs enhances the localization accuracy. Moreover, the increase in the number of ANs is shown in Fig. 8 to decrease the CRLB using RSS and TDoA

for localizing the receiver. Finally, as expected, the increase of the number of ANs is shown to increase the mapping ability by increasing the frequency of detecting all vertices. It is very clear that at least 30 ANs are needed to have a good estimation of the VANs hence the obstacle vertices.
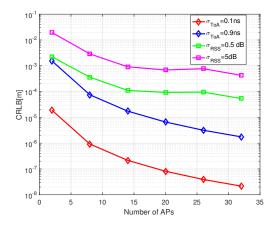

Fig. 8. CRLB of localization accuracy versus number of ANs using TDoA and RSS
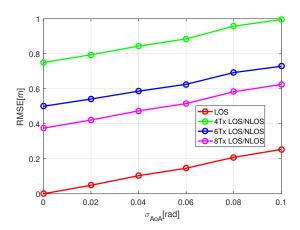

Fig. 9. RMSE versus σ_{AoA} for estimating receiver under LoS/NLoS channel

D. Obstacles Mapping

After localizing the VANs, the obstacles in the room are to be mapped in terms of their positions, dimensions and limits. Three types of obstacles have been considered: a square, a triangle and a hexagon. Fig. 10 shows the estimated vertices of a triangular obstacle in the room with $N_{Tx} = 12$ and $N_{Tx} = 42$ ANs, respectively, using the TL (ref. Section IV.A) with $\sigma_{AoA} = 0.09 rad$ ($almost 5^o$) and the K-means algorithm to cluster the set of estimated obstacle vertices. It is very clear that the TL approach presents very good accuracy if the number of ANs is large enough. Moreover, the results are in line with CRLB derived in the previous section which specifies at least 30 ANs for good accuracy. Fig. 11 and Fig. 12 present the mapping results of rectangular and hexagonal obstacles using the RSS and TDoA approaches, provided in Section IV. B and C respectively with $\sigma_{RSS} = 0.1W$ and $\sigma_{ToA} = 0.1ns$. Here, the cloud of vertices points at each measurement is shown as well as the resulting estimated vertices using K-means

algorithm. Moreover, 42 ANs were used to estimate accurately a square obstacle, as shown in Fig. 13, using the TDoA with $\sigma_{ToA} = 0.05ns$.
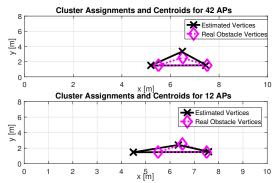

Fig. 10. Obstacle (triangle) mapping using the TL approach to estimate the VANs
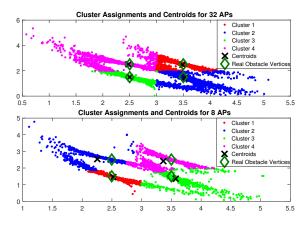

Fig. 11. Obstacle (rectangle) mapping using RSS approach

E. Analysis and Conclusions on the Simulations Results

The CRLB level of the TL, i.e. AoA, approach has shown a decrease with the increase in the number of ANs under LoS environment as shown in Fig. 9. Nevertheless, this is not the case with NLoS environment. However, as the obstacle mapping highly depends on the localization accuracy from one side and needs the reflection paths from the other side, it becomes very important to select the optimal number of ANs which is able to realize both localization and mapping. Another important resides in the AoA measurement errors as they highly affect the accuracy of the obstacle mapping. However, thanks to the large number of antennas implemented in mmWave technology, these errors are very small [30]. Similarly, TDoA is shown to achieve high accuracy in terms of localizing VANs with respect to the noise variance of the ToA measurements. In practice, the ToA based approach provides a negligible estimation error in the localization approach. However, the mapping needs an estimation of the AoA which again needs to be very accurate. In terms of raw accuracy, 10 GHz bandwidth is required to achieve accurate estimation using TDoA with an error in the order of 0.1 ns in terms of σ_{ToA}. This is indeed one advantage of using mmWave whose band can reach few GHz.

RSS based approach is the worst in terms of estimating the VANs positions due to an increased error in the Rx localization

as shown in the CRLB given in Fig. 9. Moreover, this bias is increased in practice due to the absorption loss by the obstacles on the NLoS rays powers. Finally, it is worth mentioning that the simulation results have shown that the localization and mapping within the MOSAIC framework present an excellent accuracy reaching few centimeters if appropriate parameters are selected.
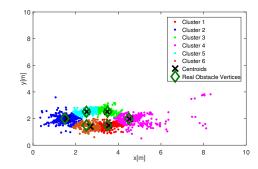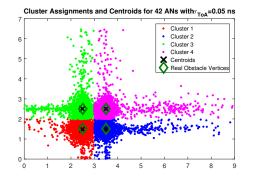

Fig. 12. Obstacle (hexagon) mapping using TDoA

Fig. 13. Effect of the increase in σ_{TDoA} on the estimation of the vertices of a square obstacle using TDoA

VII. Conclusion

In this paper, we presented MOSAIC a framework for joint localization and mapping. The concept is based on few steps based on localization of the receiver, followed by the estimation of the VANs and then obstacle mapping and dimensioning. The performance of the localization techniques is tested through simulations in terms of RMSE and CDF of the location estimation error. In terms of obstacle detection, the paper proposed a new approach based on VANs and mirroring. A thorough analysis of the proposed approaches has been made in the paper from theoretical and algorithmic point of view. It has been shown that increasing the number of ANs increases the probability of localization and obstacle detection. Simulations have shown that finding the optimal number of ANs using the CRLB is a compromise between localization and obstacle mapping accuracy. The paper consists a first of its kind in mapping an indoor environment based on the RSS, ToA and AoA measurements. Definitely, much work could be achieved in the future. Among others, the localization and detection of multiple objects is a possible future direction. Also, the localization, detection and classification (object, human, etc) of moving objects will be of order in the future research directions.

VIII. References

[1] T. Rappaport et al., *Millimeter Wave Wireless Communications*. Pearson Education, 2014.

[2] S. Rangan, T. S. Rappaport and E. Erkip, "Millimeter-Wave Cellular Wireless Networks: Potentials and Challenges," in *Proceedings of the IEEE*, vol. 102, no. 3, pp. 366-385, March 2014.

[3] A. Kupper. Location-based services. Wiley, 2005

[4] M. Bocquet, N. Obeid, C. Loyez, C. Lethien, F. Boukour, N. Rolland, and M. Heddebaut, "Comparison between 60-GHz UWB frequency modulation and UWB impulse-radio location systems", *in Radar Conference*,2008. EuRAD 2008. European, Oct. 2008, pp. 4143.

[5] H. R. Fang, G. P. Cao, E. A. Gharavol, K. Tom, and K. Mouthaan, "60 GHz short range planar RSS localization", *in Proceedings of Asia-Pacific Microwave Conference 2010*, 2010.

[6] A. Jafari, J. Sarrazin, D. Lautru, A. Benlarbi-Dela, L. Petrillo and P. De Doncker, "NLOS influence on 60 GHz indoor localization based on a new TDOA extraction approach," *2013 European Microwave Conference*, Nuremberg, 2013, pp. 330-333.

[7] L. Subrt, P. Pechac, and S. Zvanovec, "New approach to modeling of diffuse reflection and scattering for millimeter-wave systems in indoor scenarios", *PIERS Online*, vol. 6, 2010.

[8] N. Peinecke, H. Doehler, and B. Korn, "Phong-like lighting for MMW radar simulation", *in Proc. SPIE*, Cardiff, UK, 2008.

[9] A. Maltsev et al., "Experimental investigations of 60 GHz WLAN systems in office environment", *IEEE J. Sel. Areas Commun.*, vol. 27, no. 8, pp. 14881499, Oct. 2009.

[10] T. Rappaport et al., "Millimeter wave mobile communications for 5G cellular: It will work!" *IEEE Access*, vol. 1, pp. 335349, 2013.

[11] G. R. MacCartney et al., "Path loss models for 5G millimeter wave propagation channels in urban microcells", *in Proc. IEEE GLOBECOM*, Atlanta, GA, Dec. 2013.

[12] T. Rappaport et al., "Broadband millimeter-wave propagation measurements and models using adaptive-beam antennas for outdoor urban cellular communications", *IEEE Trans. Antennas Propag.*, vol. 61, no. 4, pp. 18501859, Apr. 2013.

[13] W. Morris, I. Dryanovski, and J. Xiao, "3D indoor mapping for micro-uavs using hybrid range finders and multi-volume occupancy grids," in Proc. RSS 2010 Workshop RGB-D: Adv. Reasoning With Depth Cameras, 2010.

[14] H. Durrant-Whyte and T. Bailey, Simultaneous localisation and mapping (SLAM): Part I the essential algorithms, IEEE Robotics Autom. Mag., vol. 13, no. 2, pp. 99110, Jun. 2006.

[15] M. W. M. G. Dissanayake, P. Newman, S. Clark, H. F. Durrant-Whyte, and M. Csorba, "A solution to the simultaneous localization and map building (SLAM) problem,"*IEEE Trans. on Robotics and Automation,*vol. 17, pp. 229241, 2001.

[16] A. Guerra, F. Guidi, and D. Dardari, "Position and orientation error bound for wideband massive antenna arrays," in *Proc. IEEE Int. Conf. Commun.*, ANLN Workshop, 2015.

[17] W. Hong et al., "Study and prototyping of practically Large-scale mmWave antenna systems for 5G cellular devices," *IEEE Commun. Mag.*, vol. 52, no. 9, pp. 6369, Sep. 2014.

[18] H. Kaouach et al., "Wideband low-loss linear and circular polarization transmit-arrays in V-Band," *IEEE Trans. Antennas Propag.*, vol. 59, no. 7, pp. 25132523, Jul. 2011.

[19] J. Hoydis, S. ten Brink, and M. Debbah, "Massive MIMO in the UL/DL of cellular networks: How many antennas do we need?" *IEEE J. Select. Areas Commun.*, vol. 31, no. 2, pp. 160171, 2013.

[20] E. G. Larsson, F. Tufvesson, O. Edfors, and T. L. Marzetta, "Massive MIMO for next generation wireless systems," *CoRR*, vol. abs/1304.6690,2013.

[21] F. Guidi, A. Guerra and D. Dardari, "Millimeter-wave massive arrays for indoor SLAM,"*2014 IEEE International Conference on Communications Workshops (ICC)*, Sydney, NSW, 2014, pp. 114-120.

[22] A. Guerra, F. Guidi, and D. Dardari, "Millimeter-wave personal radars for 3D environment mapping," in *Proc. IEEE Asilomar Conf. Signals, Syst. Comput.*, Pacific Grove, USA, Nov. 2014, pp. 701705.

[23] C. Wu, Z. Yang, and Y. Liu, "Smartphones based crowdsourcing for indoor localization," *IEEE Trans. Mobile Comput.*, vol. 14, no. 2, pp. 444457, Feb. 2015.

[24] A. Guerra et al., "Application of transmit array antennas for indoor mapping at Millimeter-waves," in *Proc. IEEE Eur. Conf. Netw. Commun.*, 2015, pp. 7781.

[25] F. Guidi, A. Guerra and D. Dardari, "Personal Mobile Radars with Millimeter-Wave Massive Arrays for Indoor Mapping," in*IEEE Transactions on Mobile Computing*, vol. 15, no. 6, pp. 1471-1484, June 1 2016.

[26] C. Floerkemeier, M. Langheinrich, E. Fleisch, F. Mattern, and S. E. Sarma, Eds., *The Internet of Things, First Int. Conf.* Springer, 2008

[27] H. El-Sayed, G. Athanasiou and C. Fischione, "Evaluation of localization methods in millimeter-wave wireless systems," *2014 IEEE 19th International Workshop on Computer Aided Modeling and Design of Communication Links and Networks (CAMAD)*, Athens, 2014, pp. 345-349.

[28] A. Olivier, G. Bielsa, I. Tejado, M. Zorzi, J. Widmer and P. Casari, "Lightweight Indoor Localization for 60-GHz Millimeter Wave Systems," *2016 13th Annual IEEE International Conference on Sensing, Communication, and Networking (SECON)*, London, 2016, pp. 1-9.

[29] A. Yassin, Y. Nasser, M. Awad and A. Al-Dubai, "Simultaneous context inference and mapping using mm-Wave for indoor scenarios," *2017 IEEE International Conference on Communications (ICC)*, Paris, 2017, pp. 1-6.

[30] A. Shahmansoori et al., "Position and Orientation Estimation through Millimeter Wave MIMO in 5G Systems", IEEE Trans. Wireless Commun., 2017, [online] Available: https://arxiv.org/abs/1702.01605.

[31] T. Kos, M. Grgic, and G. Sisul, Mobile user positioning in gsm/umts cellular networks, *in Multimedia Signal Processing and Communications*, 48th International Symposium ELMAR-2006 focused on, Zadar, Croatia, Jun. 2006.

[32] P. Meissner, T. Gigl, and K. Witrisal, UWB sequential monte carlo positioning using virtual anchors *in Proc. IPIN*, Zurich, Switzerland, Sep. 2010.

[33] L. Cheng, X. Wu and Y. Wang, "A non-line of sight localization method based on k-means clustering algorithm," 2017 7th IEEE International Conference on Electronics Information and Emergency Communication (ICEIEC), Macau, 2017, pp. 465-468.

Appendix: RSS-WLS solution

The aim here is to enhance the estimation taking into account the noise variance. We start with an example of 3 measurements and then the equations are updated accordingly. Equation (21) can be written as:

$$\mathbf{P}_{WLS} \cdot \mathbf{R}_{WLS} = \mathbf{T}_{WLS} \tag{55}$$

where $\mathbf{P}_{WLS}$, $\mathbf{R}_{WLS}$ and $\mathbf{T}_{WLS}$ are defined as follows:

$$\mathbf{P}_{WLS} = \begin{bmatrix} \mathbf{P}_{12}(1) & \mathbf{P}_{13}(1) & & & \\ \mathbf{P}_{12}(2) & \mathbf{P}_{13}(2) & 0 & \cdots & 0 \\ & 0 & \ddots & \vdots & \vdots \\ \vdots & & \cdots & \mathbf{P}_{12}(1) & \mathbf{P}_{13}(1) \\ 0 & & \cdots & \mathbf{P}_{12}(2) & \mathbf{P}_{13}(2) \end{bmatrix}$$

$$\mathbf{R}_{WLS} = \begin{bmatrix} 2(x_2 - x1) \\ 2(y_2 - y1) \vdots \\ 2(x_{N_p} - x1) \\ 2(y_{N_p} - y1) \end{bmatrix}$$

$$\mathbf{T}_{WLS} = \begin{bmatrix} \mathbf{T}_d(1,1) \\ \mathbf{T}_d(1,2) \vdots \\ \mathbf{T}_d(N_p - 1, 1) \\ \mathbf{T}_d(N_p - 1, 2) \end{bmatrix}$$

where $\mathbf{P}_{12} = \mathbf{p}_1^{Rx} - \mathbf{p}_2^{Rx}$ and $\mathbf{P}_{13} = \mathbf{p}_1^{Rx} - \mathbf{p}_3^{Rx}$. Additionally, knowing that the dimensions of $\mathbf{R}_{WLS}$ and $\mathbf{T}_{WLS}$ are $2 \times (N_p - 1) \times 1$ and the dimension of $\mathbf{P}_{WLS}$ is $2 * (N_p - 1) \times 2 * (N_p - 1)$. Hence, $\mathbf{P}_{WLS}$ can be written as follows:

$$\mathbf{P}_{WLS} = \mathbf{I} \otimes \begin{bmatrix} \mathbf{P}_{12}(1) & \mathbf{P}_{13}(1) \\ \mathbf{P}_{12}(2) & \mathbf{P}_{13}(2) \end{bmatrix} \tag{56}$$

where $\mathbf{I}$ is the identity matrix of dimension $(N_p - 1) \times (N_p - 1)$. Consequently, $\mathbf{R}_{WLS}$ of the VANs can be estimated by:

$$\hat{\mathbf{R}}_{WLS} = \frac{1}{2} (\mathbf{W}_{WLS} \cdot \mathbf{P}_{WLS})^{-1} \mathbf{W}_{WLS} \cdot \cdot \mathbf{T}_{WLS} \qquad (57)$$

where the weighting matrix $\mathbf{W}_{WLS}$ is equal to the inverse of the covariance matrix $\boldsymbol{\Sigma}_{WLS}$ of the vector $\mathbf{T}_{WLS}$.